Spinodal decomposition and pattern formation near surfaces

1990 J. Phys.: Condens. Matter 2 10303

(http://iopscience.iop.org/0953-8984/2/51/006)

J. Phys.: Condens. Matter 2 (1990) 10303–10320. Printed in the UK

Spinodal decomposition and pattern formation near surfaces

R C Ball and R L H Essery

Cavendish Laboratory, University of Cambridge, Madingley Road, Cambridge CB3 0HE, UK

Received 13 July 1990

Abstract. The effects of temperature gradients and boundary conditions at the surface of a system separating into two phases via spinodal decomposition are studied numerically in one and two dimensions. For suitable cooling rates and thermal noise strengths, an off-critical system cooled from an external surface is found to separate by the formation of alternate layers of the two phases near the surface, a very different structure to that formed in the bulk. A similar pattern is found to be generated by a boundary condition associated with a surface free energy. An approximate solution is derived for the evolution of the boundary pattern in this case, allowing an estimate to be made of how far the pattern will propagate into the bulk.

1. Introduction

This paper is concerned with the influence of boundary conditions and temperature gradients at a surface on the structure formed near the surface and the cross-over to the bulk structure in a system undergoing rapid phase separation. We discuss this within the framework of the Ginzburg–Landau theory of phase separation for systems in which the order parameter is a conserved quantity, such as the local concentration of one of the components in a binary alloy or polymer blend.

Typically, the phase separation is induced by quenching the system from a homogeneous, thermal equilibrium state to a non-equilibrium state below a critical temperature, T_c. This will evolve towards a new and inhomogeneous equilibrium consisting of two coexisting phases, characterized by different values of the order parameter. In the bulk, homogeneity is destroyed by the growth of fluctuations in the order parameter. However, the surface itself is a major inhomogeneity already present and may nucleate a quite different pattern of decomposition.

A loose distinction can be made between two types of instability characterizing the early stages of phase separation, depending on whether the system is quenched to a metastable or an unstable state (figure 1). A metastable state decays by the thermally activated formation and growth of droplets of the minority phase. An unstable state decays by the growth of long-wavelength fluctuations (spinodal decomposition), leading to a characteristic interconnected structure which coarsens with time.

The growth of this spinodal structure from thermal fluctuations in bulk systems following an instantaneous quench from a one-phase state has been studied extensively [1]. In section 2 we describe a commonly used model and modify it to represent the

0953-8984/90/5110303+18$03.50

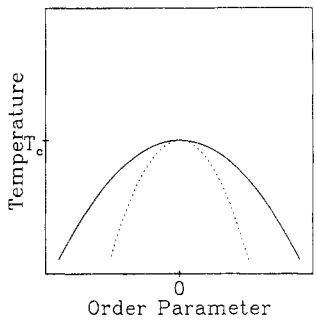

Figure 1. Phase diagram for a system which separates into two coexisting phases below a critical temperature, T_c. Points above the coexistence curve (full curve) represent stable, single phase states. States below the classical spinodal curve (dotted curve) are unstable; those between the spinodal and the coexistence curve are metastable.

more realistic situation in which the system is cooled from the outside. Numerical methods for this model are discussed and results presented in sections 3 and 4. We also consider the effects of surface free energy and compare linear analytic and numerical results for pattern propagation following an instantaneous quench.

2. The model

The model of spinodal decomposition used here is that developed by Cahn and Hilliard [2] and Cook [3]. This is a phenomenological equation for the evolution of the order parameter, $\psi(\boldsymbol{r},t)$, which, being conserved, obeys a continuity equation

$$\frac{\partial\psi(\boldsymbol{r},t)}{\partial t} = -\boldsymbol{\nabla}\cdot\boldsymbol{j}(\boldsymbol{r},t). \tag{1}$$

A linear relation is assumed between the flux, $\boldsymbol{j}$, and the gradient of the local chemical potential

$$\boldsymbol{j}(\boldsymbol{r},t) = -M\nabla\mu(\boldsymbol{r},t) \tag{2}$$

where M is the mobility, assumed to be constant. The chemical potential, μ, is given by the functional derivative of the free energy

$$\mu(\boldsymbol{r},t) = \frac{\delta F\{\psi\}}{\delta\psi(\boldsymbol{r},t)} \tag{3}$$

which is taken to have the Ginzburg–Landau form

$$F\{\psi\} = \int \mathrm{d}\boldsymbol{r}\left[f(\psi) + \tfrac{1}{2}C(\boldsymbol{\nabla}\psi)^2\right] \tag{4}$$

$$f(\psi) = \tfrac{1}{2}a\psi^2 + \tfrac{1}{4}u\psi^4. \tag{5}$$

The gradient term in equation (4) limits spatial inhomogeneities and $f(\psi)$, neglecting fluctuations, determines the equilibrium phase diagram. The parameter a can be thought of as a reduced temperature

$$a \propto \frac{T - T_c}{T_c}. \tag{6}$$

For $T > T_c, a > 0$ and $f(\psi)$ has only one minimum (figure 2), corresponding to a single equilibrium state, but for $T < T_c$ it has a double well form, the two minima giving the order parameters for the two coexisting phases,

$$\psi_{\text{coex}} = \pm \left(\frac{|a|}{u} \right)^{1/2}. \tag{7}$$

States for which $f(\psi)$ has negative curvature are locally unstable and the boundaries of this region define the classical spinodal curve,

$$\psi_{\text{spin}} = \pm \left(\frac{|a|}{3u} \right)^{1/2}. \tag{8}$$

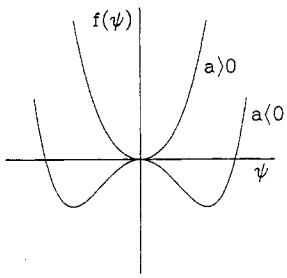

Figure 2. Free energy density for positive and negative reduced temperatures.

Equations (1)–(5) combine to give the time-dependent Ginzburg–Landau equation

$$\frac{\partial \psi(\boldsymbol{r}, t)}{\partial t} = M \nabla^2 [a\psi + u\psi^3 - C\nabla^2 \psi] + \eta(\boldsymbol{r}, t). \tag{9}$$

Thermal fluctuations [3] are represented by the inclusion of η, a Gaussian random noise term satisfying the fluctuation-dissipation theorem, in this case:

$$\langle \eta(\boldsymbol{r}, t) \eta(\boldsymbol{r}', t') \rangle = -2k_B T M \nabla^2 \delta(\boldsymbol{r} - \boldsymbol{r}') \delta(t - t'). \tag{10}$$

In theoretical studies it is generally assumed that the entire system is quenched instantaneously from above to below the critical temperature [4]. Experimentally, however, the system would be cooled from the outside by placing it in contact with a reservoir at the required final temperature and the phase separation would then begin preferentially at the boundary between the system and the reservoir. We model this quench procedure by taking the reduced temperature to be the solution of a heat diffusion equation

$$\frac{\partial a(\boldsymbol{r}, t)}{\partial t} = D \nabla^2 a(\boldsymbol{r}, t). \tag{11}$$

For a system initially at temperature $a_0 > 0$ placed in contact with a reservoir at temperature $a_1 < 0$ at $t = 0$, the initial and boundary conditions for equation (11) are

$$a(\boldsymbol{r}, 0) = a_0 \tag{12}$$

$$a(\boldsymbol{r}, t)|_{\text{boundary}} = a_1. \tag{13}$$

This also raises the question of boundary conditions for equation (9). This is not a problem when considering an infinite system, since requiring that ψ should have a transform imposes sufficient conditions. For a bounded system with conserved ψ, one obvious condition is that there should be no flux across the boundary:

$$\boldsymbol{n} \cdot \boldsymbol{\nabla} \mu(\boldsymbol{r}, t)|_{\text{boundary}} = 0 \tag{14}$$

where $\boldsymbol{n}$ is normal to the boundary. Another condition is needed to solve equation (9)—we choose to require that the gradient of ψ should vanish perpendicular to the boundary:

$$\boldsymbol{n} \cdot \boldsymbol{\nabla} \psi(\boldsymbol{r}, t)|_{\text{boundary}} = 0. \tag{15}$$

A generalization of this condition will be discussed later.

Rescaling the variables

$$\psi \rightarrow \left(\frac{|a_1|}{u}\right)^{1/2} \psi \tag{16}$$

$$\boldsymbol{r} \rightarrow \left(\frac{C}{|a_1|}\right)^{1/2} \boldsymbol{r} \tag{17}$$

$$t \rightarrow \frac{C}{M a_1^2} t \tag{18}$$

equations (9)–(11) can be put in the dimensionless forms [5]

$$\frac{\partial \psi(\boldsymbol{r}, t)}{\partial t} = \nabla^2 \left(\frac{a}{|a_1|}\psi + \psi^3 - \nabla^2 \psi\right) + \sqrt{\epsilon}\mu(\boldsymbol{r}, t) \tag{19}$$

$$\langle \mu(\boldsymbol{r}, t)\mu(\boldsymbol{r}', t')\rangle = -\nabla^2 \delta(\boldsymbol{r} - \boldsymbol{r}')\delta(t - t'), \tag{20}$$

$$\frac{\partial a(\boldsymbol{r}, t)}{\partial t} = \beta \nabla^2 a(\boldsymbol{r}, t) \tag{21}$$

where

$$\epsilon = \frac{k_B T u}{a_1^2} \left(\frac{|a_1|}{C}\right)^{d/2} \tag{22}$$

and

$$\beta = \frac{D}{|a_1| M}. \tag{23}$$

It can now be seen that, apart from scale factors, the only parameters in this model are the average order parameter (ψ_0), the noise strength (ϵ), the ratio of the initial and final temperatures ($a_0/|a_1|$) and β, which reflects the ratio of the thermal diffusion and the order parameter mobility.

For the equilibrium properties of the system to be well approximated by mean-field theory, the Ginzburg criterion requires that ϵ should be small. Note from equation

(22) that $\epsilon = 0$ corresponds to the zero-temperature limit and that ϵ diverges near the critical point ($a_1 \to 0$) for $d < 4$.

The non-linear nature of equation (19) and the coupling between the order parameter and temperature fields precludes an analytic solution, but some insight can be gained by solving for small fluctuations about ψ_0, the average order parameter, at constant temperature [2]. Introducing $\phi(\boldsymbol{r},t) = \psi(\boldsymbol{r},t) - \psi_0$, equation (19) becomes

$$\frac{\partial \phi(\boldsymbol{r},t)}{\partial t} = \nabla^2 \left(\frac{a}{|a_1|} + 3\psi_0^2 - \nabla^2 \right) \phi(\boldsymbol{r},t) + \sqrt{\epsilon}\mu(\boldsymbol{r},t) \tag{24}$$

for small ϕ. This has the Fourier transform

$$\frac{\partial \phi(\boldsymbol{k},t)}{\partial t} = -k^2 \left(\frac{a}{|a_1|} + 3\psi_0^2 + k^2 \right) \phi(\boldsymbol{k},t) + \sqrt{\epsilon}\mu(\boldsymbol{k},t). \tag{25}$$

A linear evolution equation for the structure function, defined by

$$S(\boldsymbol{k},t) = \langle |\phi(\boldsymbol{k},t)|^2 \rangle \tag{26}$$

can be derived from equations (20) and (25):

$$\frac{\partial S(\boldsymbol{k},t)}{\partial t} = -2k^2 \left(\frac{a}{|a_1|} + 3\psi_0^2 + k^2 \right) S(\boldsymbol{k},t) + \epsilon k^2. \tag{27}$$

For $a > 0$, this has an equilibrium solution of Ornstein–Zernicke form,

$$S(k) = \frac{\epsilon}{2[a/|a_1| + 3\psi_0^2 + k^2]} \tag{28}$$

which tends to zero at high temperature.

For $a = a_1$ below the spinodal curve, equation (27) can be written as

$$\frac{\partial S(\boldsymbol{k},t)}{\partial t} = 2k^2(k_c^2 - k^2)S(\boldsymbol{k},t) + \epsilon k^2 \tag{29}$$

with $k_c^2 = 1 - 3\psi_0^2 > 0$, which has the solution

$$S(\boldsymbol{k},t) = \left(S(\boldsymbol{k},0) + \frac{\epsilon}{2(k_c^2 - k^2)} \right) \mathrm{e}^{2\omega t} - \frac{\epsilon}{2(k_c^2 - k^2)} \tag{30}$$

where the amplification factor, $\omega(k) = k^2(k_c^2 - k^2)$, is positive for wavenumbers less than k_c and is peaked at $k = k_m = k_c/\sqrt{2}$. Neglecting fluctuations in the intermediate states ($\epsilon = 0$), linear theory thus predicts that fluctuations in the initial state with wavenumbers less than k_c will grow exponentially after a quench below T_c, the fastest growing being those with wavenumber k_m, independent of time. Short-wavelength fluctuations are suppressed.

The above analysis neglects non-linear effects. Various theoretical [5,6] and computational [7,8] schemes have been proposed to approximate the non-linear evolution of $S(\boldsymbol{k},t)$ as determined by equation (19). The main conclusions to be drawn are that the growth of the unstable modes slows down as equilibrium values of the order parameter are approached, and that k_m, the wavenumber at which the structure function is peaked, decreases with time—this is the coarsening mentioned earlier. The linearized solution, equation (30), is only valid at early times, if at all.

3. Numerical technique

Numerical solutions were sought for equation (19) using a technique based on that used by Petschek and Metiu [7] and Rogers *et al* [8]. The system is represented by a lattice of spacing h and the time is split into discrete steps of length Δt. We use the notation

$$\psi_i(n) = \psi(\boldsymbol{r}_i, t_n) \tag{31}$$

where $\boldsymbol{r}_i$ is a lattice point and $t_n = n\Delta t$.

Finite-difference approximations are used for both the temporal and spatial derivatives:

$$\frac{\partial \psi(\boldsymbol{r}_i, t_n)}{\partial t} \approx \frac{\psi_i(n) - \psi_i(n-1)}{\Delta t} \tag{32}$$

$$\nabla^2 G[\psi(\boldsymbol{r}_i, t_n)] \approx \frac{1}{h^2} \sum_{nn} G[\psi_i(n)] \tag{33}$$

the nearest-neighbour sum being defined by

$$\sum_{nn} G[\psi_i(n)] = \sum_j \{G[\psi_{i+j}(n)] - G[\psi_i(n)]\} \tag{34}$$

where $\boldsymbol{r}_{i+j} = \boldsymbol{r}_i + \boldsymbol{r}_j$, $\boldsymbol{r}_j$ a nearest-neighbour lattice vector. Equation (19) is thus replaced by

$$\psi_i(n+1) = \psi_i(n) + \frac{\Delta t}{h^2} \sum_{nn} \left(\frac{a_i(n)}{|a_1|} \psi_i(n) + \psi_i(n)^3 - \frac{1}{h^2} \sum_{nn} \psi_i(n) \right) + \mu_i'(n) \tag{35}$$

where

$$\mu_i'(n) = \sqrt{\epsilon} \int_{t_n}^{t_{n+1}} \mu(\boldsymbol{r}_i, t')\, \mathrm{d}t'. \tag{36}$$

The noise strength is assumed to be near enough constant over the temperature range of the quench. From equation (20),

$$\langle \mu_i'(m) \mu_j'(n) \rangle = -\epsilon \Delta t \delta_{mn} \nabla^2 \delta(\boldsymbol{r}_i - \boldsymbol{r}_j). \tag{37}$$

Replacing ∇^2 by its finite-difference approximation and the Dirac delta by a product of Kronecker deltas, this becomes

$$\langle \mu_i'(m) \mu_j'(n) \rangle = \begin{cases} 2d\epsilon h^{-2} \Delta t \delta_{mn} & \boldsymbol{r}_i = \boldsymbol{r}_j \\ -\epsilon h^{-2} \Delta t \delta_{mn} & \boldsymbol{r}_i, \boldsymbol{r}_j \text{ nearest neighbours} \\ 0 & \text{otherwise.} \end{cases} \tag{38}$$

In 2D, this can be realized by generating two independent Gaussian distributed random numbers, $\nu^{(1)}$ and $\nu^{(2)}$, at each lattice point, labelled by (i, j), with covariances

$$\langle \nu_{ij}^{(a)}(m) \nu_{kl}^{(b)}(n) \rangle = \epsilon \Delta t \delta_{ab} \delta_{ik} \delta_{jl} \delta_{mn} \tag{39}$$

and taking

$$\mu'_{ij} = \frac{1}{h}(\nu^{(1)}_{i+1,j} - \nu^{(1)}_{ij} + \nu^{(2)}_{i,j+1} - \nu^{(2)}_{ij}) \tag{40}$$

at each time step.

Some care must be taken in the choice of h and Δt to avoid spurious solutions of equation (35) with no analogue in the continuous equation (19). A linear stability analysis of equation (35) without the noise term for an instantaneous quench reveals that the following stability condition is required [8]:

$$\Delta t < \frac{h^4}{8d^2 - 2dh^2}. \tag{41}$$

We discretize the thermal diffusion equation, (21), similarly, to give

$$a_i(n+1) = a_i(n) + \frac{\beta \Delta t}{h^2} \sum_{nn} a_i(n) \tag{42}$$

with the further stability condition

$$\Delta t < \frac{h^2}{2d\beta}. \tag{43}$$

Equations (35) and (42) now provide a prescription for finding the order parameter and temperature at time $t = (n+1)\Delta t$ from known results at $t = n\Delta t$, Δt being chosen to satisfy condition (41) or (43), whichever is the more restrictive.

4. Results and discussion

Simulations were performed on a 2D lattice of 50 x 50 sites with periodic boundary conditions at the top ($y = 50h = L$) and bottom ($y = 0$) and boundary conditions at the left ($x = 0$) and right ($x = L$) edges taken from equations (14) and (15):

$$\left.\frac{\partial \mu}{\partial x}\right|_{x=0,L} = 0 \tag{44}$$

$$\left.\frac{\partial \psi}{\partial x}\right|_{x=0,L} = 0. \tag{45}$$

Initial states with an equilibrium distribution of fluctuations were prepared by "annealing' states with constant $\psi = \psi_0$ for a period at the initial temperature, a_0. The system was then cooled from the left-hand edge, the boundary conditions on the temperature field being

$$a|_{x=0} = a_1 \tag{46}$$

$$\left.\frac{\partial a}{\partial x}\right|_{x=L} = 0. \tag{47}$$

The right-hand boundary condition, equation (47), is chosen so that no effects due to a temperature gradient are generated there. Note that the temperature is independent

of y. The initial and final temperatures are chosen to be symmetric above and below T_c, $a_1 = -a_0$.

Typical simulation results for an instantaneous quench ($\beta = \infty$) at slightly off-critical composition ($\psi_0 = 0.1$—well within the spinodal region) with low noise ($\epsilon = 10^{-4}$) are presented in figures 3(a)-(c), where lattice points at which $\psi > \psi_0$ have been shaded. From an initial state with small fluctuations about ψ_0, patches with higher and lower order parameters evolve, forming a characteristic weaving, interconnected structure which grows with time. By time $t = 100$ after the quench, the system has separated into domains in which the order parameter is close to the equilibrium values of ± 1, with quite sharp walls between them.

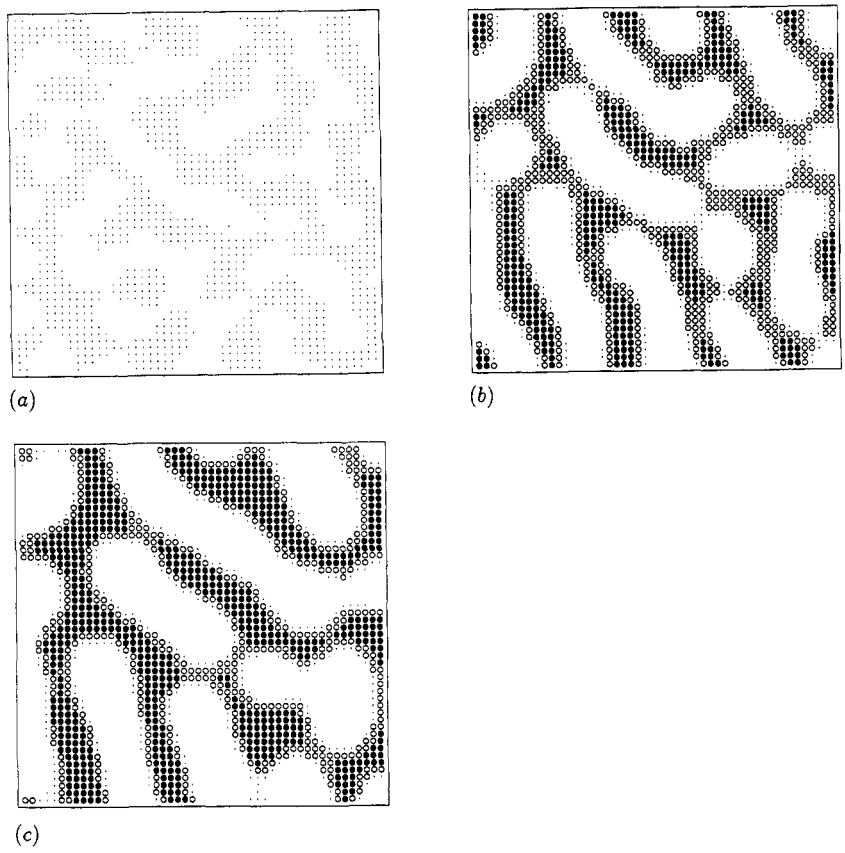

Figure 3. Evolution of the order parameter with time, t, in an off-critical ($\psi_0 = 0.1$) 2D simulation with $\epsilon = 10^{-4}$, following an instantaneous quench at time $t = 0$. (a) $t = 10$, (b) $t = 50$, (c) $t = 100$. Lattice points at which $\psi > \psi_0$ are shaded as follows: ·, $\psi_0 < \psi < 0.5$; ○, $0.5 < \psi < 0.8$; ●, $\psi > 0.8$.

If, instead of quenching instantaneously, a slightly off-critical system is cooled slowly from one edge, a very different structure is formed. Results for the same initial state as above, slowly cooled ($\beta = 10$) from the left-hand edge are shown in figure 4. At first, a layer with $\psi > \psi_0$ forms at the cooled boundary (figure 4(a)). The fluctuations in the bulk are small and disperse. As the cooling progresses, the density at the boundary increases and a second layer of enhanced ψ appears (figure 4(b)). Later still, a third layer appears (figure 4(c)), and so on. It can be seen that as this layered

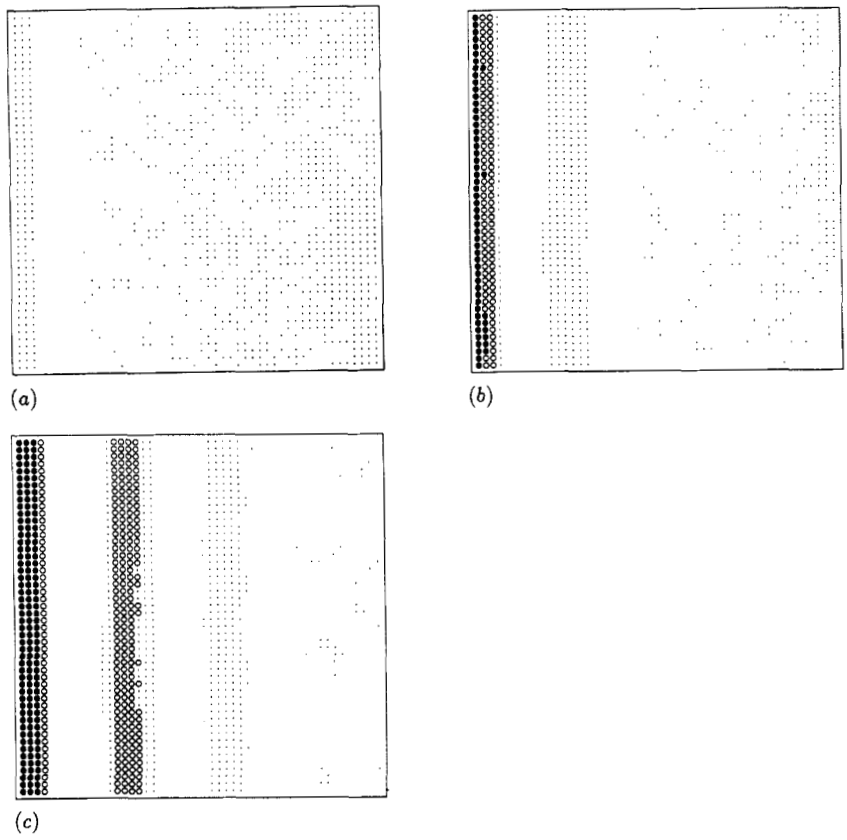

Figure 4. Evolution of an off-critical 2D simulation cooled from the left-hand boundary with slow thermal diffusion; $\psi_0 = 0.1$, $\beta = 10$, $\epsilon = 10^{-4}$. (*a*) $t = 10$, (*b*) $t = 50$, (*c*) $t = 100$.

structure advances into the bulk, the spacing between the layers stretches slightly and no separation occurs ahead of the leading layer.

The pattern of phase separation propagating from the boundary can be more clearly seen in the results of a 1D, deterministic simulation—since the temperature field is uniform in the y direction, the pattern it generates is essentially one dimensional. For $\beta = 10$, the cooling is sufficiently slow that the leading edge of the pattern is 'stuck' behind the temperature front (figure 5). Thermal fluctuations, if present, are suppressed ahead of the front and the boundary pattern can propagate far into the bulk. If the system is cooled faster, the temperature front can outrun the propagating pattern. This is seen for the case $\beta = 100$ in figure 6. The pattern now reaches further into the system at any time, but a region ahead of the pattern is cooled below the spinodal point and thermal fluctuations would nucleate phase separation there.

Returning to the 2D stochastic model, figure 7 shows that a pattern still propagates from the boundary for $\beta = 100$, but phase separation proceeds ahead of the pattern and there is a cross-over between the boundary pattern and standard spinodal decomposition in the bulk. Note that the spacing between the layers is now less than that for the slower quench and is in fact very close to the most unstable wavelength for an instantaneous quench.

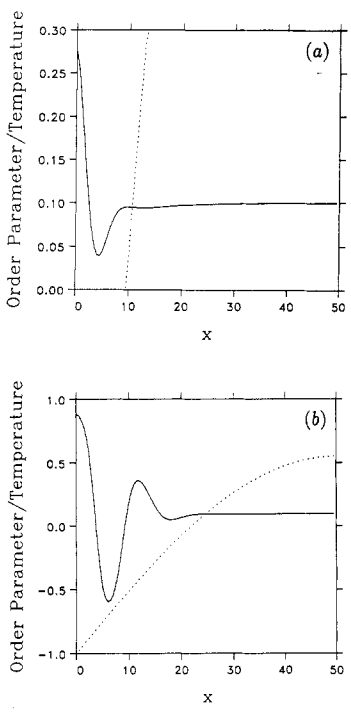

Figure 5. Order parameter (full curve) and temperature (dotted curve) in a noiseless ($\epsilon = 0$) 1D simulation for the same conditions as figure 3: $\psi_0 = 0.1$, $\beta = 10$. (*a*) $t = 10$, (*b*) $t = 50$.

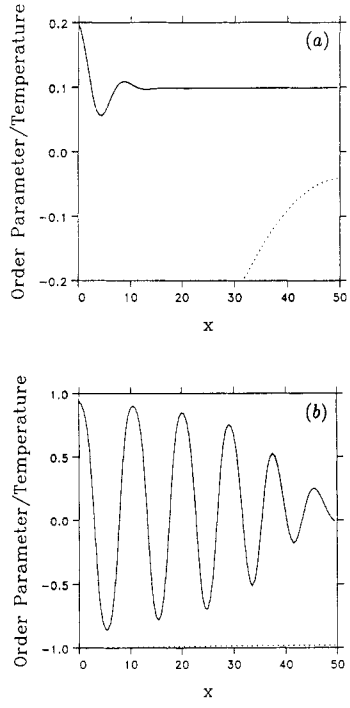

Figure 6. Order parameter (full curve) and temperature (dotted curve) in a noiseless ($\epsilon = 0$) 1D simulation with faster thermal diffusion; $\psi_0 = 0.1$, $\beta = 100$. (*a*) $t = 10$, (*b*) $t = 50$.

Increasing the noise strength to $\epsilon = 10^{-3}$, the layers formed by slow cooling are roughened, but retain their integrity (figure 8(*a*)). For the faster cooling rate, however, thermally nucleated spinodal decomposition is now dominant right up to the boundary and no vestige of the layered structure can be seen (figure 8(*b*)).

The generation of a pattern propagating from a cooled boundary can be understood by considering a flat initial state on which a temperature gradient is imposed. This forces an initial flux

$$\boldsymbol{j} = -\frac{\psi_0}{|a_1|}\nabla a. \tag{48}$$

The system is cooled from the outside and so ∇a is normal to the boundary, pointing inwards. For $\psi_0 > 0$ there is thus a flux towards the boundary, but no flux is allowed out and so ψ increases in a layer around the boundary. Conservation requires that ψ be depleted beyond this layer (figure 5(*a*)). As the temperature front advances, the depleted region is cooled below the spinodal point and the thermodynamic instability drives a flux against the gradient of ψ, consolidating the boundary layer and forming a second layer further inside the system (figure 5(*b*)). In this way, a standing wave is generated, the envelope of which advances into the system behind the temperature front.

Our model free energy is symmetric between the high and low order parameter phases and so, if one phase is to be preferentially formed at the boundary, the initial

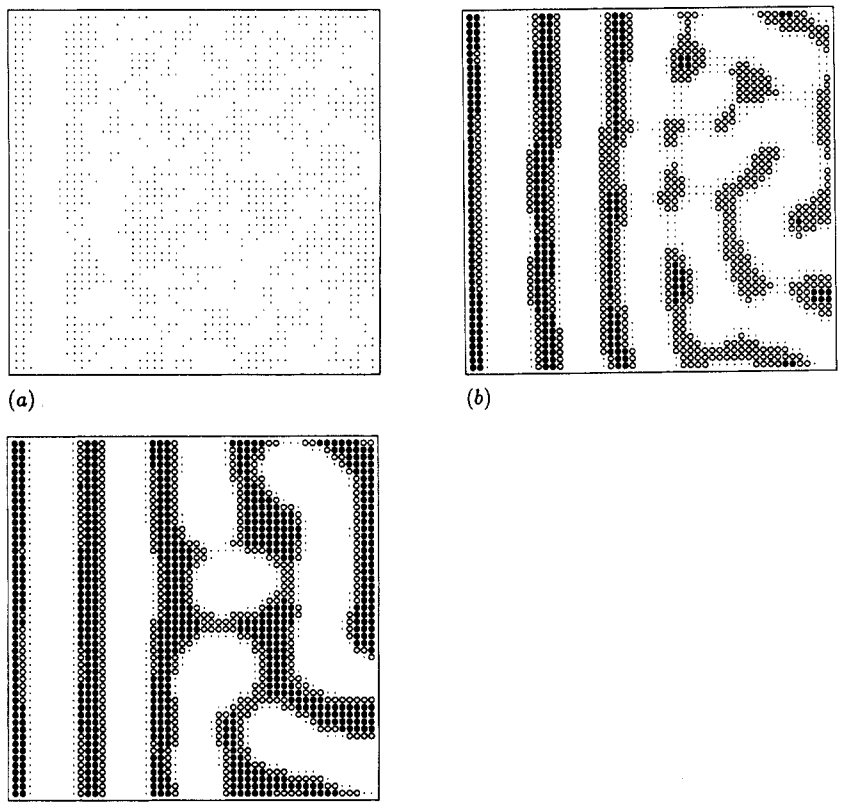

Figure 7. Evolution of an off-critical 2D simulation cooled from the left-hand boundary with faster thermal diffusion and noise; $\psi_0 = 0.1$, $\beta = 100$, $\epsilon = 10^{-4}$. (*a*) $t = 10$, (*b*) $t = 50$, (*c*) $t = 100$.

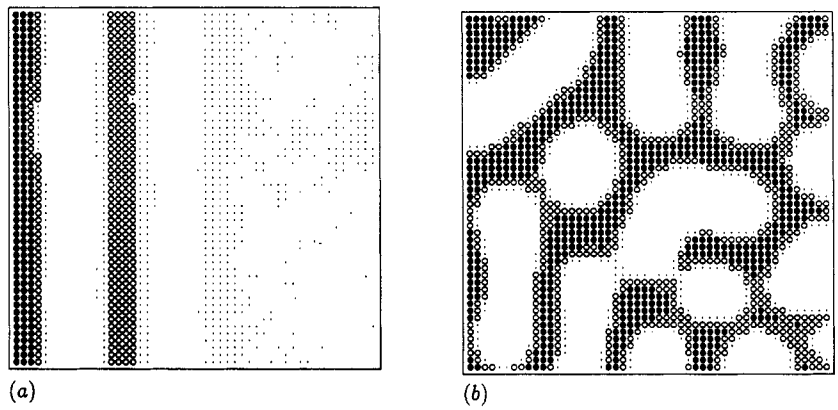

Figure 8. Effect of increasing noise strength to $\epsilon = 10^{-3}$ in 2D simulations with $\psi_0 = 0.1$. (*a*) Slow cooling ($\beta = 10$) from the left-hand boundary at $t = 100$; cf figure 4(*c*)—layered structure is preserved. (*b*) Faster cooling ($\beta = 100$) from the left-hand boundary at $t = 100$; cf figure 7(*c*)—layered structure is not preserved.

conditions must break this symmetry—ψ_0 must be non-zero (off-critical). The phase formed at the boundary is that which has the same sign as ψ_0.

The temperature gradient produced by slow cooling, the no-flux boundary condition and the asymmetry of the initial state are crucial for the generation of the layered structure observed in figure 4. A no-flux boundary condition was a natural choice for our model, but the other necessary condition, equation (15), was chosen on an *ad hoc* basis—a more general boundary condition is discussed in the next section.

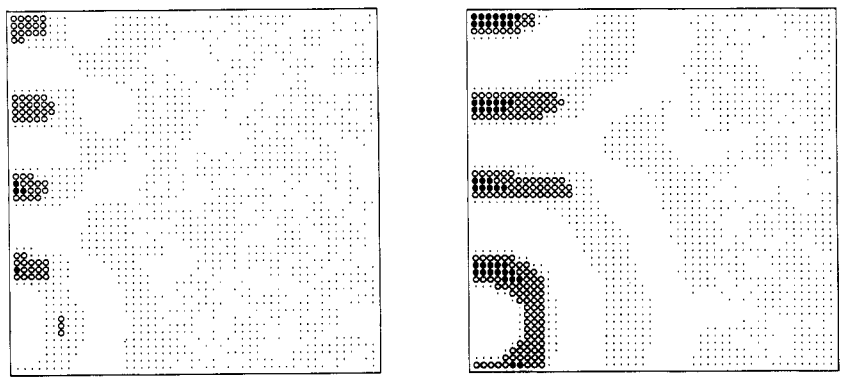

(*a*) (*b*)

Figure 9. Evolution of a critical 2D simulation cooled from the left-hand boundary with slow thermal diffusion; $\psi_0 = 0$, $\beta = 10$, $\epsilon = 10^{-4}$. (*a*) $t = 50$, (*b*) $t = 100$.

An instantaneous quench produces qualitatively similar results whether the initial state is symmetric on the average ($\psi_0 = 0$) or slightly asymmetric, but slow cooling produces a different type of structure. Figure 9(*a*) shows results for a symmetric initial state, slowly cooled from the left-hand edge. Patches of both phases now appear at the cooled boundary (figure 9(*a*)), developing into concentric, semi-circular bands centred on the boundary (figure 9(*b*)). It should be noted that this pattern is thermally nucleated, whereas the layered pattern of figure 4 represents a deterministic solution of the model equation, in competition with thermal fluctuations.

5. Surface free energy

So far, it has been assumed that the surface makes no contribution to the free energy. We now add a surface term

$$F\{\psi\} = F_{\text{bulk}} + \tfrac{1}{2}\alpha \int \psi^2 \, \mathrm{d}s \tag{49}$$

where F_{bulk} is the bulk free energy from equation (4) and the integral is over the surface of the system. The functional derivative of equation (49) gives the bulk chemical potential as before and the same Ginzburg–Landau equation, equation (19), is recovered, but the surface term now supplies an equilibrium boundary condition

$$[\boldsymbol{n} \cdot \boldsymbol{\nabla}\psi(\boldsymbol{r}, t) + \alpha\psi(\boldsymbol{r}, t)]_{\text{boundary}} = 0. \tag{50}$$

We adopt this as a generalization of boundary condition (15) for the dynamics. Since the surface free energy may induce surface segregation even in the absence of a temperature gradient, we consider instantaneous quenches only. The early stages of phase separation neglecting thermal noise can be studied using the linearized evolution equation, (24), with $\epsilon = 0$. For a 1D semi-infinite system ($0 < x < \infty$), this is

$$\frac{\partial \phi(x,t)}{\partial t} = -\frac{\partial^2}{\partial x^2}\left(k_c^2 + \frac{\partial^2}{\partial x^2}\right)\phi(x,t). \tag{51}$$

where $k_c^2 = 1 - 3\psi_0^2$. The boundary conditions at $x = 0$ are

$$\frac{\partial \phi(0,t)}{\partial x} + \alpha[\phi(0,t) + \psi_0] = 0 \tag{52}$$

and

$$\frac{\partial}{\partial x}\left(k_c^2 + \frac{\partial^2}{\partial x^2}\right)\phi(0,t) = 0 \tag{53}$$

and for a flat initial state the initial condition is

$$\phi(x,0) = 0. \tag{54}$$

The neglect of thermal fluctuations and surface segregation in the initial state correspond to taking a very high initial temperature.

Taking a Fourier cosine transform in x and a Laplace transform in t, the transform of $\phi(x,t)$ is

$$\phi(k,s) = \int_0^\infty \mathrm{d}t\, \mathrm{e}^{-st} \int_0^\infty \mathrm{d}x\, \phi(x,t) \cos kx \tag{55}$$

$$= \frac{\alpha k^2}{s - \omega(k)}\left(\frac{\psi_0}{s} + \frac{2}{\pi}\int_0^\infty dk_1\, \phi(k_1,s)\right) \tag{56}$$

from equation (51), where

$$\omega(k) = k^2(k_c^2 - k^2). \tag{57}$$

Equation (56) is an integral equation for $\phi(k,s)$ with solution

$$\phi(k,s) = \frac{\alpha\psi_0 k^2}{s(s-\omega)}\left(1 - \frac{2\alpha}{\pi}\int_0^\infty \frac{k_1^2\, \mathrm{d}k_1}{s - \omega(k_1)}\right)^{-1}. \tag{58}$$

The integral in equation (58) could be evaluated, but to avoid a messy inverse Laplace transform we restrict our attention to small values of α and retain the first-order term only:

$$\phi(k,s) \approx \frac{\alpha\psi_0 k^2}{s(s-\omega)}. \tag{59}$$

Inverting the Laplace transform,

$$\phi(k,t) \approx \alpha\psi_0 k^2 \frac{e^{\omega t} - 1}{\omega} \tag{60}$$

and inverting the Fourier transform,

$$\phi(x,t) \approx \frac{2\alpha\psi_0}{\pi} \int_0^\infty dk \, \frac{\exp\{k^2(k_c^2 - k^2)t\} - 1}{k_c^2 - k^2} \cos kx. \tag{61}$$

Equation (61) can be evaluated approximately, noting that the integrand is sharply peaked near $k = k_m = k_c/\sqrt{2}$ and using a Gaussian approximation, to give

$$\phi(x,t) \approx \frac{\alpha\psi_0}{k_m^3\sqrt{\pi t}} \exp\left(k_m^4 t - \frac{x^2}{16k_m^2 t}\right)\left(A\cos k_m x - \frac{x}{4k_m^3 t}\sin k_m x\right) \tag{62}$$

where

$$A = 1 + \frac{5}{8k_m^4 t}\left(1 - \frac{x^2}{8k_m^2 t}\right). \tag{63}$$

This is compared with the results of a 1D simulation in figure 10. The agreement is good for small α and ϕ.

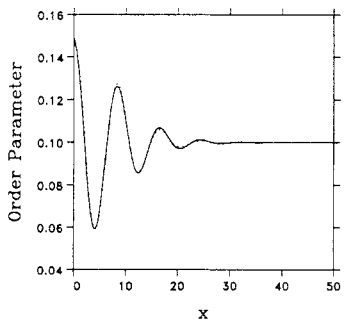

Figure 10. Boundary pattern induced by surface energy effects at the left-hand boundary in 1D at time $t = 20$ after an instantaneous quench with $\psi_0 = 0.1$, $\alpha = 0.1$ and $\epsilon = 0$. Full curve from simulation, dotted curve from equation (62).

If α and ψ_0 are both non-zero, a damped standing-wave pattern is generated, the envelope of which decays into the bulk. Equation (62) predicts that wavenumber k_m is strongly selected and that the velocity at which the envelope advances tends to a constant value, $v \to 4k_m^3$, at large times.

This situation belongs to a class of problems in which a pattern of well defined wavelength is formed behind a front propagating into a uniform, unstable state for which 'marginal stability' [9–11] has been suggested as a dynamical pattern selection mechanism.

At the leading edge of the pattern, displacements about ψ_0 are small and the linearized equation, (51), will be valid. At large times and far away from the location of any initial perturbation, this has solutions of the form

$$\phi(x,t) \sim \exp(ikx + \omega(k)t) \tag{64}$$

the amplification rate, ω, being given by the linear dispersion relation, equation (57). Requiring $\mathrm{Im}\, k > 0$, the envelope of this solution decays with increasing x and advances at velocity

$$v = \frac{\mathrm{Re}\,\omega(k)}{\mathrm{Im}\, k}. \tag{65}$$

A solution exists for *any* front velocity, but the marginal stability hypothesis states that the naturally selected velocity of the front is such that slower moving fronts, viewed in a co-moving frame, are unstable against perturbations, while faster moving fronts are stable, or

$$v = \mathrm{i}\frac{\mathrm{d}\omega(k)}{\mathrm{d}k}. \tag{66}$$

Equations (65) and (66) can be solved simultaneously for v and k, the wavenumber of the small fluctuations ahead of the front. The wavenumber for the pattern emerging behind the front is given by

$$k^* = \frac{\mathrm{Im}\,[\mathrm{i}kv + \omega(k)]}{v}. \tag{67}$$

With ω from equation (57), the marginal stability predictions for this problem are [12]

$$v = \frac{4(\sqrt{7}+2)}{3}\left(\frac{\sqrt{7}-1}{3}\right)^{1/2} k_{\mathrm{m}}^3 \approx 4.588 k_{\mathrm{m}}^3 \tag{68}$$

$$k^* = \frac{3(\sqrt{7}+3)^{3/2}}{8(\sqrt{7}+2)} k_{\mathrm{m}} \approx 1.083 k_{\mathrm{m}} \tag{69}$$

in reasonable agreement with the approximate predictions above.

In 2D simulations with thermal noise, a cross-over can again be seen between an essentially one-dimensional pattern propagating from the boundary and fully two-dimensional, thermally nucleated spinodal decomposition in the bulk (figure 11).

A linear theory for the growth of thermal fluctuations in the bulk was discussed in section 2. Following an instantaneous quench from a flat (high-temperature) stable state to an unstable state, equation (30) predicts that

$$\langle \phi^2(t) \rangle = \frac{\epsilon}{4\pi} \int_{-\infty}^{\infty} \mathrm{d}k \frac{\mathrm{e}^{2\omega t} - 1}{k_{\mathrm{c}}^2 - k^2} \tag{70}$$

which can be evaluated using the same approximation as for equation (62):

$$\langle \phi^2(t) \rangle \approx \frac{\epsilon}{4k_{\mathrm{m}}^3\sqrt{2\pi t}} \left(1 + \frac{5}{16k_{\mathrm{m}}^4 t}\right) \exp(2k_{\mathrm{m}}^4 t). \tag{71}$$

This is compared with simulation results in figure 12. A good fit is obtained for small ϕ, but non-linear effects begin to be important at about $\phi = 0.2$.

An estimate of how far the boundary pattern will reach into the bulk can be made since at early times the competing processes of pattern propagation and thermally nucleated spinodal decomposition are described by a linear equation and can

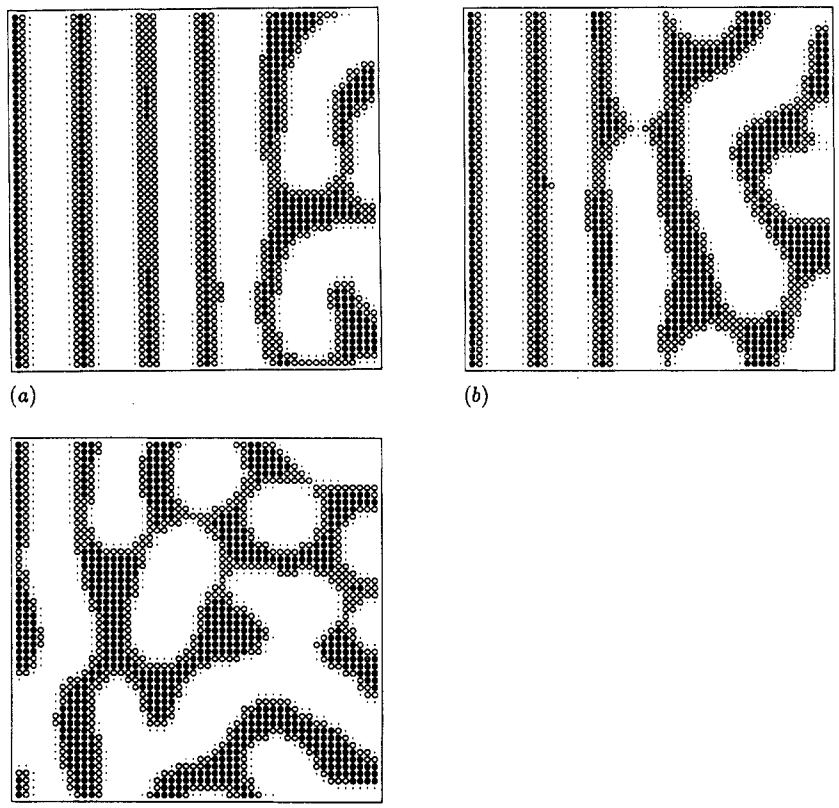

Figure 11. Off-critical ($\psi_0 = 0.1$) 2D simulations at time $t = 100$ after an instantaneous quench for various strengths of the surface interaction and the noise: (*a*) $\alpha = 0.1$, $\epsilon = 10^{-8}$; (*b*) $\alpha = 0.1$, $\epsilon = 10^{-6}$; (*c*) $\alpha = 0.01$, $\epsilon = 10^{-6}$.

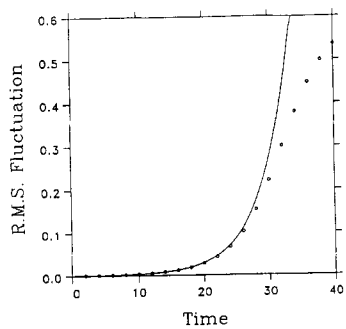

Figure 12. Growth of RMS fluctuation, $\langle\phi^2(t)\rangle^{1/2}$, for thermally nucleated spinodal decomposition with $\psi_0 = 0.1$ and $\epsilon = 10^{-6}$. Full curve from linear theory (equation (70)), points from simulation.

be superimposed, but when their sum reaches the non-linear regime in some region, whichever is larger will remain dominant in that region subsequently. Choosing a non-linear threshold (we take $\phi = 0.2$, but the results are insensitive to the exact choice)

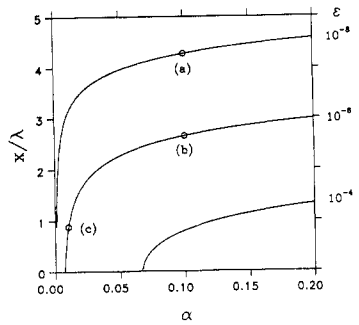

Figure 13. Predicted distance from boundary for cross-over between boundary pattern and bulk decomposition in pattern wavelengths, $\lambda = 2\pi/k_m$, plotted against surface interaction strength (α) for three different noise strengths (ϵ). Marked points (a)–(c) correspond to parameters for figures 11(a)–(c).

and comparing equation (71) with the envelope part of equation (62), a rough prediction can be made for the distance from the boundary over which the boundary pattern will dominate bulk decomposition. This distance, in terms of pattern wavelengths, is plotted against α for various noise strengths in figure 13. The marked points (a)-(c) correspond to the parameters for the simulations shown in figures 11(a)–(c).

For $\psi_0 = 0.1$, $\epsilon = 10^{-8}$ and $\alpha = 0.1$, the pattern is expected to extend for a little more than four wavelengths from the boundary. This corresponds to figure 11(a), in which four distinct dark bands (positive ϕ) can be seen and a fifth (four wavelengths) merges into the bulk pattern. Similarly, the pattern in figure 11(b), predicted to extend for about 2.5 wavelengths, shows three distinct dark bands while the next unshaded band (negative ϕ) is nearly, but not quite, complete. In figure 11(c) the first band is incomplete, the second is greatly roughened and bulk spinodal decomposition is dominant beyond one wavelength from the boundary.

6. Conclusions

We have seen how boundary conditions can dictate that one phase should be preferentially formed at the boundary of a system with a symmetric phase diagram undergoing separation into two phases, provided that the initial state is not symmetric between the two phases (i.e. that it is off-critical). It is then a general property of the mathematical model used that alternate layers of the two phases will be formed near the boundary.

In the first case studied, a flux of one phase towards the boundary was generated by a temperature gradient due to cooling of the boundary. The observation of a boundary pattern is favoured in systems which have an appreciable material mobility compared with their thermal conductivity (i.e. small β). However, hydrodynamic effects, neglected here, might be important.

For the more common case in which the thermal conductivity is large compared with the material mobility (large β), the instantaneous quench assumption becomes a good approximation. However, surface energy effects are then important and we have shown that these can also lead to layered boundary patterns.

Boundary layers, if formed, could give the surface quite different physical properties to the bulk and could be probed by scattering experiments.

Acknowledgments

One of us (RLHE) would like to thank the SERC for a studentship.

References

[1] For a review, see Gunton J D, San Miguel M and Sahni P S 1983 *Phase Transitions and Critical Phenomena* vol 8, ed C Domb and J L Lebowitz (London: Academic)
[2] Cahn J W and Hilliard J E 1958 *J. Chem. Phys.* **28** 258
[3] Cook H E 1970 *Acta. Metall.* **18** 297
[4] Spinodal decomposition induced by a slow, but still homogeneous, quench has been investigated by Carmesin H O, Heerman D W and Binder K 1986 *Z. Phys.* B **65** 89
[5] Grant M, San Miguel M, Viñals J and Gunton J D 1985 *Phys. Rev.* B **31** 3027. Note, however, that their scaled time is twice ours.
[6] Langer J S, Bar-on M and Miller H D 1975 *Phys. Rev.* A **11** 1417
[7] Petschek R and Metiu H 1983 *J. Chem. Phys.* **79** 3443
[8] Rogers T M, Elder K R and Desai R C 1988 *Phys. Rev.* B **37** 9638
[9] Dee G and Langer J S 1983 *Phys. Rev. Lett.* **50** 383
[10] Ben-Jacob E, Brand H R, Dee G, Kramer L and Langer J S 1985 *Physica* D **14** 348
[11] van Saarloos W 1987 *Phys. Rev. Lett.* **58** 2571; 1988 *Phys. Rev.* A **37** 211
[12] Liu F and Goldenfeld N 1989 *Phys. Rev.* A **39** 4805